Effects of Porosity on High Strength Aluminum 7039

Porosity reduces both weld metal ductility and fatigue life but does not significantly affect yield strength

BY R. J. SHORE AND R. B. McCAULEY

SUMMARY. This paper reports on a study of the effects of porosity on the mechanical properties of high strength aluminum weldments. Gas metal-arc butt welds containing various amounts of porosity produced by moisture additions to the helium shielding gas were made in $^1/_2$ in. thick A.A. 7039-T6151 aluminum with $^1/_{16}$ in. diameter 5039 filler metal. The results of mechanical tests performed on test coupons removed from the welded plates (naturally aged at least 30 days) were related to the amount of porosity present as determined by fracture surface analyses.

Experimental results indicate that porosity reduces the transverse tensile strength of the weld metal an amount proportional to the area of sound metal lost in the region tested, i.e., the plane of maximum loss in cross section. In this study, the yield strength of the weld metal was not significantly affected by porosity. The ductility of the aluminum weld metal, as determined by percentage elongation measurements in tension tests. was sharply reduced by the presence of small amounts of porosity. Fatigue life at high stress levels was markedly reduced by small amounts of porosity—these pores acting as sites for crack initiation and growth. Sonic fatigue test work indicates that fatigue testing at 10,000 Hertz with the P-11 transducer offers many advantages over conventional type (low speed) fatigue tests.

Introduction

One of the major discontinuities in aluminum welding is porosity. Engineering evaluation of porosity in weld joints has been a serious problem since the beginning of aluminum fusion welding technology.

Weld defects such as porosity have grown more and more important as higher and higher strength alloys have been developed for applications ranging from pressure vessels, treated in the American Society of Mechanical Engineering codes, to space vehicles, as noted by National Aeronautical and Space Administration specifications. Because of this growing importance, numerous studies have been undertaken concerning the causes, prevention, and evaluation of porosity in weld joints. Even with the knowledge obtained from these studies, porosity is still frequently encountered in aluminum fusion welding.

To what level porosity can be safely accepted in an aluminum weldment is a question that must be answered for economical and reliable design. An understanding of the effects of porosity on the mechanical properties of the weldment will provide a basis to answer this question. There has been limited research in this area and thus develops the need for a study such as this. The purpose of the investigation described in this paper was to determine the effects of porosity on the mechanical properties of the high strength, aluminum-zinc-magnesium alloy 7039.

Porosity Formation

In general, porosity in weld metal is formed by the entrapment of evolved gases in the solidifying weld metal. The mechanism of this formation has been shown by Saperstein, Prescott, and Monroe to be one of nucleation and growth.[1] Their conclusion was based upon the observed dependence of porosity concentration on the apparent cooling rate of welds in A. A. 3003 using 1100 filler metal and upon the existence of a critical shielding-gas dew point below which the gas metal-arc welds deposited were virtually free of porosity. A quantitative description of porosity formation in terms of nucleation and growth rates was later provided by Saperstein and Pollack.[2]

Hydrogen is the principal cause of porosity in aluminum welds. Voids or porosity which, in general, are spherical in shape are caused by the sharp decrease in solubility of hydrogen during solidifaction. Hydrogen solubility in molten aluminum is more than ten times the solubility in solid metal. Aluminum alloying additions influence porosity formation by affecting the solubility of hydrogen in the matrix. Additions of over 3% copper, for example, markedly reduce the solubility of hydrogen in aluminum. Magnesium additions considerably increase the solubility of hydrogen in aluminum—6% magnesium almost doubling the solubility. Alloying additions also influence porosity formation in aluminum weld metal by affecting the solidification range[3] and solidification mode.[4]

The reaction of water vapor with molten aluminum to produce nascent hydrogen and the release of hydrogen from hydrogen-containing-compounds present in or near the intense heat of the arc are major souces of hydrogen which result in porosity. Souces of these hydrogen contaminants relative to gas metal arc or gas tungsten-arc welding may be grouped under the base or filler metal, surface of the base or filler metal, and the shielding gas.

Prior Investigations of the Effects of Porosity

Mechanical properties of weld metal may be adversely affected by discontinuities such as porosity because of the loss in cross-sectional area and the stress concentration associated with these defects. Stress analyses for a spherical pore and for a long cylindrical cavity in a homogeneous, elastic body of infinite length which is under a uniform tensile stress show stress concentrations of only 2.05 and 3, respectively, at the edge of the cavities.[5, 6] Nearly all weldable engineering materials have the ability to absorb or redistribute local stress concentrations of this magnitude.

Masubuchi[6] discusses the effects of defects such as porosity on the behavior of ductile material under tensile loading. In such a material, large plastic deformation occurs before fractures. Plastic regions are formed in those areas stressed above the yield

R. J. SHORE is a Graduate Research Assistant and R. B. McCAULEY is Professor and Chairman of the Department of Welding Engineering, The Ohio State University, Columbus, Ohio.

Paper presented at the 51st Annual Meeting held in Cleveland, Ohio. during June 8-12, 1970.

Table 1—Chemical Composition of Alloy 7039, %

Si	0.3 max	Cr	0.15 to 0.25
Fe	0.4 max	Zn	3.5 to 4.5
Cu	0.1 max	Ti	0.1 max
Mn	0.1 to 0.4	Others	0.05 to 0.15
Mg	2.3 to 3.3	Aluminum	remainder

point. This plastic deformation reduces the stress concentrations around the defect. Thus, weld joint mechanical property losses associated with porosity do not result directly from the stress concentrations around these pores. Masubuchi notes that fracture in such ductile materials is by shear failure, usually occurs when the net stress approaches the ultimate tensile stress, and propagates relatively slowly.

If the reduction of strength due to porosity is determined by the loss in cross-sectional area, a pore size which gives the least ratio of cross-sectional area to volume is to be desired. As noted by Martin investigators,[7] from a consideration of the ratio of cross-sectional area to volume for a spherical pore, a given volume of contaminant gas in a freezing puddle can cause more damage (area reduction) in the form of small pores than large pores. In the Martin study an observed sudden loss in tensile strength with low levels of porosity (only pores $\geq {}^{1}/_{64}$ in. diameter counted) in gas tungsten-arc welds with 2219-T87 using 2319 filler metal and with 2014-T6 using 4043 filler metal was attributed largely to uncounted fine porosity. In later work at Martin, however, Rudy and Rupert[8] evaluated this fine porosity; they concluded that the loss in transverse tensile strength of the aluminum weld metal was proportional to the loss of sound metal area in the plane of expected fracture.

A porosity study in the static case by Green, Hamad and McCauley,[9] indicated up to 7% porosity could be tolerated in mild steel welds (40,000 psi yield stress) with no loss of original properties. A similiar study by Bradley and McCauley[10] with 100,000 psi yield strength steel showed a loss of cross-section up to 5-6% may be present with original plate properties obtained.

Baysinger[11] showed with gas metal-arc welds of aluminum alloy 5083 welded with 5356 filler metal that considerable porosity can be tolerated before there is much effect on mechanical properties. In a study by Dinshdale and Young,[12] it was concluded that large pores have a more serious effect than fine pores—particularly in thin material, but that the tolerance to porosity is high enabling realistic acceptance criteria to be applied without detriment to static strength. Results of this study were for porosity in gas metal-arc welded Al-Mg alloys. The authors note that a consistent relationship exists between ultimate tensile strength and ductility for a given alloy. Defects which seriously affect strength have a similar deleterious effect on ductility.

Data about effects of porosity on the fatigue properties of welded materials are very limited. In the study by Rupert and Rudy,[8] fatigue life, traverse tension-tension load, showed a linear degradation in stress to failure at a given cycle life, this reduction being proportional to area loss in the fracture plane. Earlier work at Martin-Marietta,[7] with the same material, (${}^{1}/_{64}$ in. diameter only pores evaluated) showed fatigue life was markedly affected by porosity level. Young and Dinsdale,[12] in their study of the effects of uniform porosity on Al-Mg weldments, conducted tension fatigue tests (zero to maximum load) with both reinforcements left on and removed. In fatigue tests with reinforcements left on, all the failures occurred from the edge of the weld reinforcement, the porosity having no effect. Limited test results of welds with the reinforcement removed indicated that the position of the discontinuities rather than the magnitude of site is the principle criterion. Also the fatigue strength is critically dependent on the presence of pores breaking the surface, or just under the surface.

Research Program

Materials

Aluminum alloy A. A. 7039 is a heat treatable, weldable, aluminum-zinc-magnesium alloy. The alloy was developed for armor-plate applications, but its high strength, weldability, formability, toughness, and corrosion resistance have made it useful for cryogenic and general structural applications. Robinson and Baysinger[13] report that typical mechanical properties of A. A. 7039-T6151 plate are 58,000 psi tensile strength, 48,000 psi yield strength and 14% elongation. A. A. 7039-T64 plate properties are 65,000 psi tensile strength, 55,000 psi yield strength and 13% elongation. Mechanical property data from Battelle Memorial Institute[14] show alloy A. A. 7039 base metal and weldments have good low-temperature toughness and mechanical properties for cryogenic applications down to −320°F. The chemical composition of the alloy is shown in Table 1.

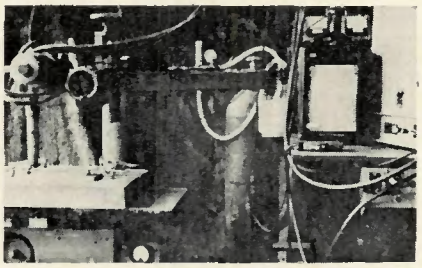

Fig. 1—View of welding set-up

Table 2—Chemical Composition of Alloy 5039, %

Si	0.10 max	Cr	0.10 to 0.20
Fe	0.40 max	Zn	2.4 to 3.2
Cu	0.03 max	Ti	0.10 max
Mn	0.03 to 0.50	Be	0.0008 max
Mg	3.3 to 4.3	Others	0.10 max
		Aluminum	remainder

With the development of the weldable alloy A.A. 7039, Kaiser Aluminum and Chemical Corporation found it necessary to develop a filler metal to more fully utilize the strength advantage of the plate than was possible with existing Al-Mg filler metals. Gibbs[15] describes the development of A. A. 5039 from weld tensile strength data and cruciform crack test data of welds made with various filler metal compositions. The final composition that produced satisfactory combination of strength and freedom from cracks is shown in Table 2.

Robinson and Baysinger[13] and Liptak[16] report in studies of the weldability of alloy A. A. 7039 using A. A. 5039 filler metal that the alloy is readily welded with gas tungsten-arc or gas metal-arc processes. Mechanical properties after natural aging weldments 15 to 30 days at 70 to 75° F. were approximately 50,000 psi tensile strength and 30,000 psi yield strength with 10% elongation.

Welding

To study the effects of porosity on the mechanical properties of aluminum weld metal, gas-metal-arc welds were made joining ${}^{1}/_{2}$ in. thick plates of the high-strength aluminum alloy 7039-T6151. The filler metal was 5039, ${}^{1}/_{16}$ in. diameter.

The as-received 7039 plate sections were cut to the welded plate dimensions of 6 by 12 in. For uniformity, all plates were cut such that the rolling direction would be perpendicular to the welding direction. After cutting, plate edges to be welded were machined with a shaper. A double-vee butt joint with a ${}^{1}/_{16}$ in. root face and 70 deg included angle was utilized. Immediately prior to welding, prepared plate edges were brushed with a stainless steel wire brush, with 0.0104 in. diameter wire. Plates were clamped in welding position on a 3 in. thick aluminum slab. A view of the welding set-up is shown in Fig. 1.

The welding procedure developed for joining the 7039 material consisted

of tacking the positioned plates at both ends and making a single-pass weld on each side of the double-vee butt joint. This joint preparation was determined as part of the welding procedure development. To prevent melt-through, the weld heat input was lower for the first side than for the second. Plates were allowed to cool after making the first weld pass to a temperature less than 150° F before welding on the second side of the joint. Welding parameters were recorded for all test plates. Welding procedure for joining test plates is shown in Table 3.

Once a sound welding procedure had been developed, methods of producing porosity were investigated. These included using contaminated filler metals (e.g., surface oxides and hydrocarbons present), hydrogen additions to the shielding gas, and moisture additions to the helium shielding gas. The latter method proved most successful and was used almost entirely as the means of producing various amounts of porosity. These moisture additions were made simply by bubbling part of the helium shielding gas through water in the flask shown in Fig. 1. Two sources of helium, each with regulator and flowmeter, permitted mixing of the pure helium and moisture contaminated helium in various proportions.

Table 3—Welding Procedure for Joining Test Plates

First pass
Current, amp—230 +10 −30
Voltage, v—24 ± 2
Travel, ipm—16½ ± ½
Second pass
Current, amp—270 +15 −30
Voltage, v—25 ± 2
Travel, ipm—16½ ± ½
Interpass temperature less than 150° F.
Torch stand-off distance—⅜ in.
Contact tip to work distance—½ in.
Shielding gas—100% helium, 50 to 80 cfh.

Testing

To study the effects of porosity on the mechanical properties of the aluminum weld metal, naturally aged for a minimum of 30 days, test specimens were removed transverse to the welding direction from the welded plates for tensile, impact, and fatigue tests. Specimens for these tests are shown in Fig. 2.

Load-displacement recordings of each tensile test were recorded with a 2 in. extensometer centered across the weld. Gage marks, 1 and 2 in. gage lengths, were also centered across the weld on the second-pass side of each tensile specimen. Strain rate for tensile tests was approximately 0.1 ipm. Information calculated for tensile specimens included the ultimate tensile strength—the maximum load divided by the original cross-sectional area, the yield strength—load at 0.2% offset of the load-displacement recording divided by the original cross-sectional area, and the percentage elongations—ratio of change in gage length, to nearest 0.01 in., divided by the original gage length. Change in page length was measured with the fracture surfaces closely fitted together.

Charpy specimens were tested to give an indication of the effects of porosity on the resistance of the weld metal to impact loading. Close tolerances were maintained on all specimen dimensions as shown in Fig. 2. To test as much of the weld as possible, the width of the specimen was increased from the standard 0.394 in. to 0.458—maximum possible with existing Manslab Tester at Wright Patterson Air Force Base (WPAFB). Charpy specimens were precracked in fatigue, 7000 to 10,000 cycles, to a depth of approximately 0.050 in. The energy absorbed during fracture of each specimen was recorded to the nearest 0.01 ft-lb. This value was converted to in.-lb and divided by the fractured area to give the parameter in.-lb/in^2. Effects of porosity on this parameter were determined.

Tension-tension fatigue testing, 25,000 psi maximum—1250 psi minimum, of weld metal samples taken transverse to the welding direction was done on a 20 ton, dynamic resonance type loading, Schenck fatigue machine at WPAFB. Fatigue rate of the sinusoidal, axially directed, loading was 1800 cycles/min. Specimens were milled to rough dimensions and finished by sanding and hand polishing to insure a smooth surface, except for pores breaking the surface, with no transverse finishing marks.

Sonic Testing

In addition to this conventional low frequency fatigue test, a high frequency sonic fatigue test was developed to study the effects of porosity on the fatigue life of weld metal and to simply introduce the use of the P-11 sonic transducer for fatiguing specimens. Loading rates of 10,000 Hertz offer the advantage of speed for long life fatigue studies and also actual simulation of service conditions for materials in acoustic equipment, certain parts of aircraft structures, etc., which are alternately stressed at these high rates.

The 15 horsepower (10 kw) P-11 transducer or motor, designed in the

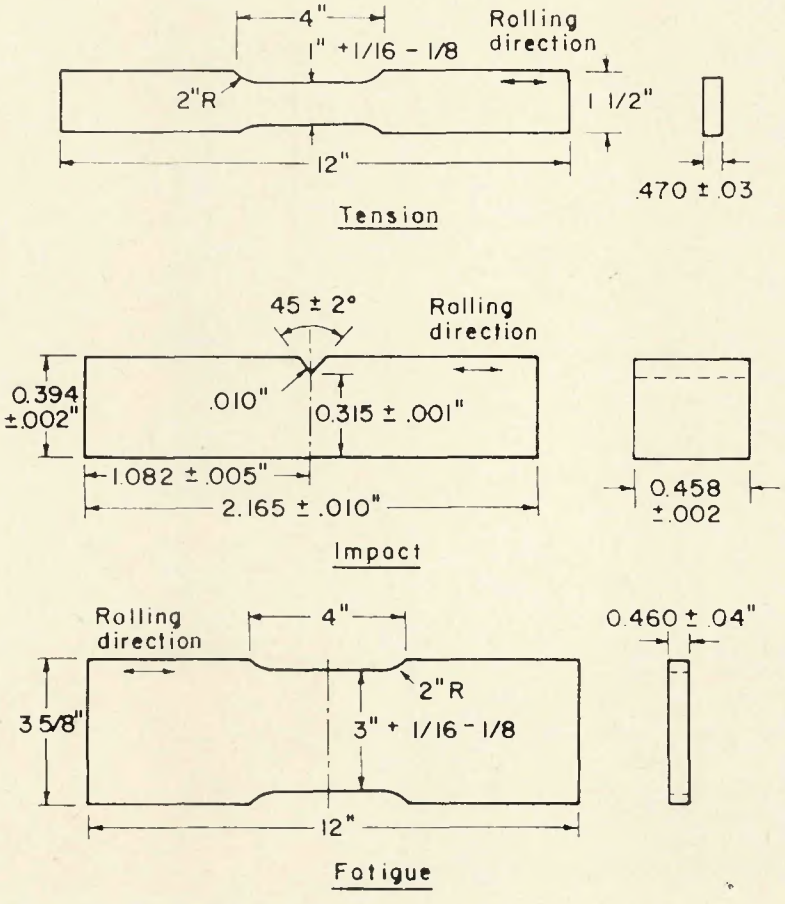

Fig. 2—Tensile, impact and fatigue test specimens

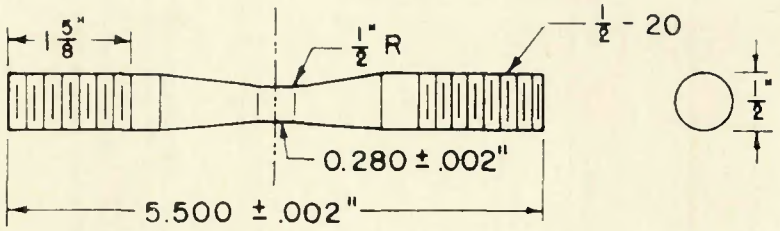

Fig. 3—Sonic fatigue specimen

Sonic Power Laboratory of the Department of Welding Engineering, delivers its power from a volume of active piezoelectric material of only $5^1/_3$ cu. in. Four lead zirconate titanate rings, mounted mechanically in series and electrically in parallel, make up the driving element. The catenoidal shaped "horn" of the full wavelength transducer amplifies the mechanical displacement of the disks and acts as a force concentrator. The mechanical displacement of the disks is varied by changing the magnitude of the voltage applied across the rings. The typical operating frequency (resonance) of a P-11 is near 10,000 Hz, with the half power frequency range of any single transducer being less than ± 10 Hz. Transducers may be manufactured with identical frequencies for coupling in motor-generator sets and for operation from the same, constant frequency power source. The power source used in these tests, however, was the variable frequency, 10 kw generator at The Ohio State University Sonic Power Laboratory. With this generator, maximum available output voltage to the transducer crystals was approximately 3000 v.

Considerable research was done in the area of sonic fatigue to develop this test. The final set-up employed two P-11 transducers, one as the driver or motor and the second simply as part of the resonant system—its crystals being short circuited. The transducers were coupled by a test specimen, refer to Fig. 3. The test samples were removed transverse to the welding direction with the weld centered in the uniform reduced section. Specimens were threaded on each end so as to screw into the $^1/_2$ in. deep hole of the transducer end. Tapered steel coupling nuts helped transmit the energy from the 1 in. diameter transducer end to the $^1/_2$ in. diameter aluminum sample and also prevented the sample from backing out of the threaded hole during operation. It was necessary to reduce the cross section at the middle of the test sample to obtain the high stress levels required for fatiguing. The final length of the sample was determined by trial and error such that the sample size and length, together with the coupling nuts, provided a half-wave length coupling between the transducers—permitting them to operate at their natural resonant frequency. The resonant system was supported at four points so the test sample experienced essentially zero static force.

The test specimens were fatigued by operating the driver transducer at the resonant frequency of the system with an applied R.M.S. signal of 600 v across each crystal. The resonance point was found by varying the frequency to minimize the input voltage to the transducer, i.e., minimize the input impedance. During the tests, the power input, voltage, and time were recorded with an oscillograph. Frequency was monitored with an electrical frequency counter. Foil strain gages were mounted on several samples to determine the stress levels at various operating voltages. An oscilloscope was used to monitor these stress levels. The frequency of the varying stress was accurately determined by measuring the oscillating d-c output of the bridge amplifier (2 arm bridge, one active gage) with the frequency counter. Figures 4 and 5 show a sample mounted in the transducer and a view of the testing equipment.

To compare the toughness of the

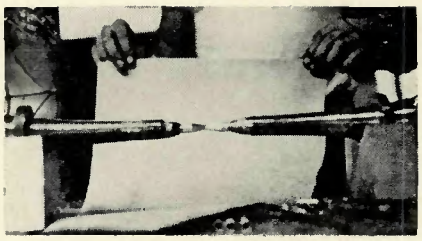

Fig. 4—Sonic fatigue sample in P-11 transducer and illustrative sketch

A. A. 7039-T6151 base metal, sound weld metal, and porous weld metal, center notch fracture specimens were tested at the Air Force Materials Laboratory at WPAFB. Fracture specimens were in accordance with recommendations of the E-24 ASTM Committee on Fracture Testing of High Stength Metallic Materials except for the length requirement where welded specimen lengths were limited to 12 in. The fracture specimen is shown in Fig. 6. These welded samples were removed from the second pass side of the welded plates. Equipment limitations did not permit the use of a $^1/_2$ in. thick sample. Surfaces of the specimen were belt sanded and then hand polished to the final close tolerances. The first part of the crack was cut with a hacksaw. A razor edge was used to sharpen the crack tip before fatigue cracking. Fatigue crack lengths were approximately the same as the thickness of the specimen.

All specimens were fatigue cracked in 12,000 to 16,000 cycles to a target total crack length of 0.45W in the 20 ton Schenck fatigue machine described above. Fracture testing was done on a 50,000 lb capacity Wiedemann-Baldwin Universal Testing machine with a head travel speed of 0.01 ipm. Load-displacement recordings of each test were made using a compliance gage positioned on knife edges across the crack in the center of the sample and taking the unbalance sig-

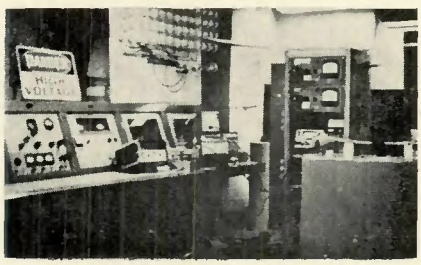
Fig. 5—Sonic fatigue testing equipment

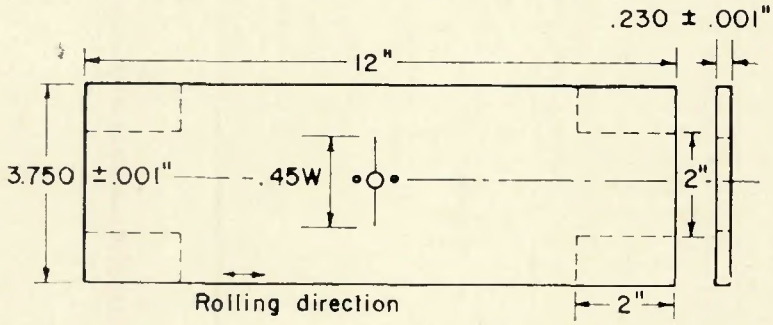

Fig. 6—Center-notch fracture specimens

nal from the amplifier of the 4 arm bridge circuit to the x-axis of an autographic recorder. Calibrations of the compliance gage output and loading signal were made for each test specimen.

Porosity Evaluation

In the investigation of the effects of porosity on mechanical properties of aluminum weld metal, the amounts of porosity in fractured specimens were determined in terms of the loss in cross-sectional area of the fracture surfaces. All experimental results presented are related to this loss in area due to porosity. In terms of nondestructive evaluation technique, considerable radiography was done to determine amounts of porosity in welds and for correlation with the fracture surface analysis. A radiograph positive of four tensile specimens is shown in Fig. 7.

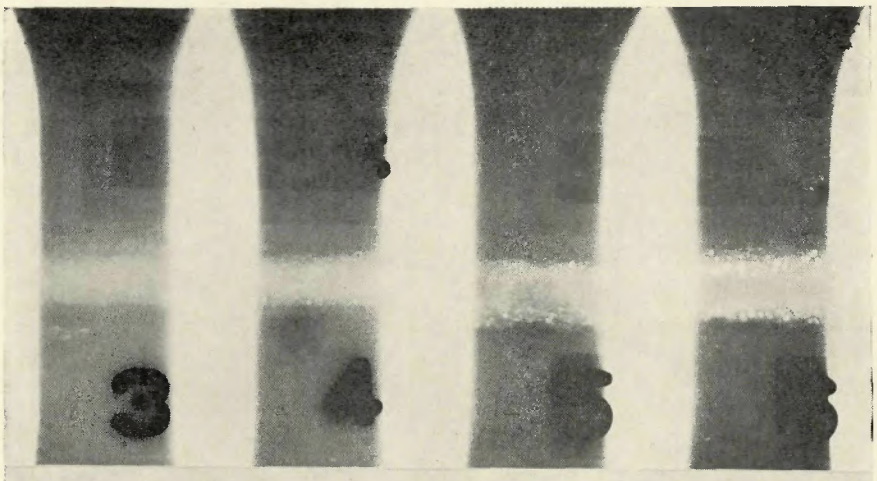

Fine Porosity (≤ 1/64"D.)	1%	6%	11%	11%
Coarse Porosity (>2/64"D.)	0%	0%	5%	10%
Total Porosity	1%	6%	16%	21%
Tensile strength ksi	49.2	42.6	36.5	30.7
Yield strength ksi	33.3	30.9	31.9	29.3

Fig. 7—Radiograph positive of four tensile specimens, Kodak film, 1½ min exposure, 65 kv, 36 in. focal-film distance

In the fracture surface analysis, pores greater than $^1/_{64}$ in. in diameter were evaluated by measuring and counting individual pores under a X10 hand microscope or from a X20 view of the fracture surface on a closed-circuit TV. The depth of focus of the special TV camera lens permitted viewing the entire fracture of most specimens without refocusing. Fracture surfaces were viewed in a direction parallel to the test specimen length. The diameters of apparently spherical porosity on these viewed surfaces were measured to the nearest $^1/_{64}$ in. for pores $^2/_{64}$ in. diameter and greater. Areas of irregularly shaped pores were approximated from measurements of width, length, etc. of the pore. A percentage area loss of an entire fracture surface due to these large pores was calculated using the original cross-sectional area of the specimen.

Pores with a diameter $^1/_{64}$ in. and less were evaluated under X30 using a microscope with a vernier scale embossed on one eyepiece. With this magnification, pores $^1/_{128}$ and $^1/_{256}$ in. in diameter were readily detectable. At this magnification, however, the entire sample could not be viewed as with the X20 TV screen. For this reason a series of views were taken across each fracture surface. These were viewed in a direction parallel with the test specimen length, to evaluate the loss in area in terms of pores $^1/_{64}$, $^1/_{128}$, and $^1/_{256}$ in. in diameter. Actual counts of pores in this area were made for each view. The vernier on the eyepiece aided in this evaluation. Pores greater than approximately $^{1.5}/_{64}$ in. in diameter were not considered as fine porosity in this analysis. The percent area loss due to these fine pores was calculated for each X30 view with respect to the total area viewed. For a $^1/_2$ in. thick tensile specimen, three such views were made across the thickness and the average loss in area of the three views was considered the loss in area due to fine porosity ($\leq$ $^1/_{64}$ in. diameter) for the entire surface. This method assumes uniform distribution of fine porosity along the length of a welded plate but not with thickness of the welded joint—a valid assumption with methods of uniform contamination. The total loss in are due to

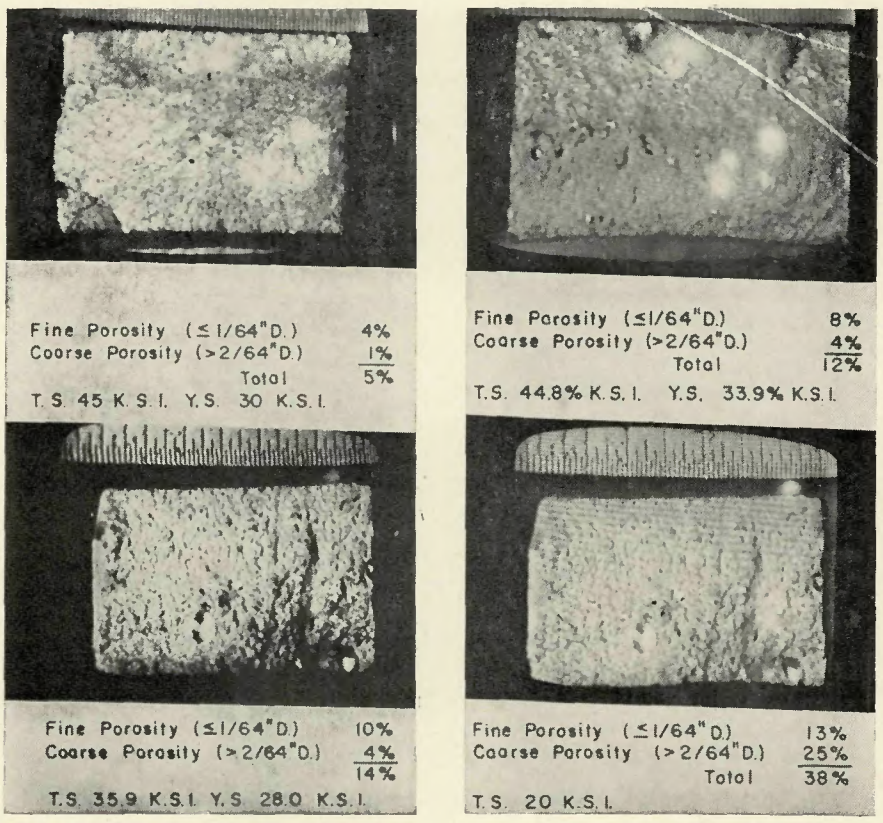

Fig. 8—Photographs of tension specimen fracture surfaces from TV screen images

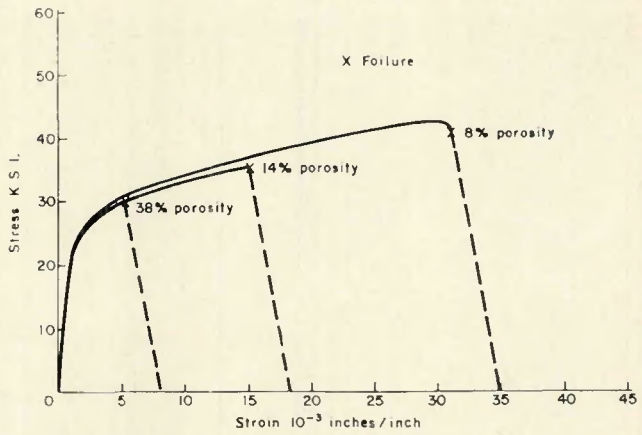

Fig. 9—Tension test engineering stress-strain curves

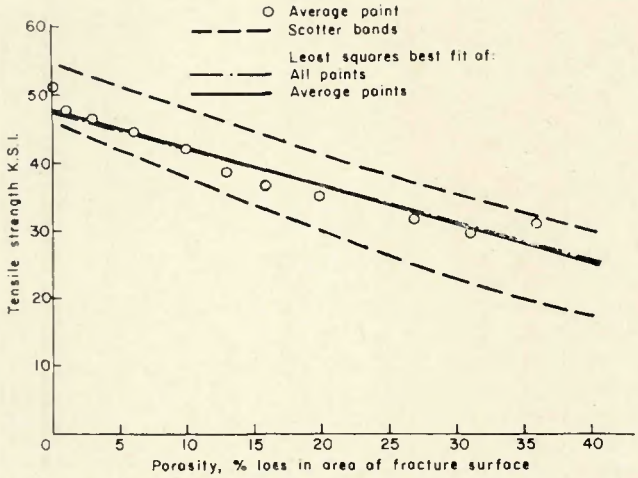

Fig. 10—Tensile strength vs. porosity

porosity for each specimen was the sum of this loss from fine pores ($\leq {}^{1}/_{64}$ in. diameter) and the loss from large pores ($\geq {}^{2}/_{64}$ in. diameter).

This method of evaluation was very time consuming but considered relatively accurate for the range of porosity investigated. Verification of the accuracy of evaluation of large and fine pores was made by comparing results of separate analyses of the same sample and also, for large pores, by tracing pores on the enlarged image of fracture surfaces. Slides were made from pictures of the TV screen images for this analysis. Paper cut-outs were weighed to determine the area loss from pores $\geq {}^{2}/_{64}$ in. in diameter. Photographs of several porous fracture surfaces are shown in Fig. 8.

Results and Discussion

Tension Testing

Several stress-strain curves for tensile samples containing various amounts of porosity are shown in Fig. 9. For tensile samples containing little or no porosity, necking occurred as illustrated by the load dropping off before fracture, i.e., the change with strain in load-carrying ability becomes less than the change in load. This necking behavior in characteristic of very ductile materials. The stress-strain curves for the tensile specimens containing 14 and 38% porosity show less ductility than the 8% porous sample and no necking behavior—the ultimate strength is the fracture strength.

The change in ultimate tensile strength with increasing porosity, represented by loss in area of the fracture surface, is shown in Fig. 10. Results show a nearly linear loss in strength with porosity. This is in agreement with earlier discussion of effects of porosity. The least squares best fit straight lines of all points and of the average points are shown in Fig. 10. The equation for the least squares best fit line of the average points is:

$$\text{Tensile strength} = 47.9 - 0.609\ (\%\ \text{loss in area}).$$

The average tensile strength of sound weld metal, 0% porosity, was 51.2 ksi, slightly higher than the intercept for this best fit straight line. Each point plotted in Fig. 10 represents the average of at least five and in some cases, as many as eleven points.

From the results, it is seen that 10 and 20% loss in strength occurs with approximately 3 and 11% porosity, respectively, if the average sound weld metal strength is taken as 51.3 ksi. With the least squares best fit straight line of the average points, the Y-intercept is 47.9 ksi. Using this value for the tensile strength of sound weld metal, 10 and 20% loss in strength occurs with approximately 8% and 16% porosity respectively. With respect to loss in area, 10 and 20% porosity reduces the tensile strength to approximately 42 and 36 ksi respectively.

The yield strengths, 0.2% elongation, as a function of porosity are shown in Fig. 11. Scatter bands and average points are plotted as in Fig. 10. Yield strength is relatively unaffected by significant amounts of porosity as indicated by the slope of the straight line. These results indicate that porosity, over the range investigated, has little effect on the elastic behavior of the material.

Loss in ductility with porosity is indicated by the elongations, two and one inch gage lengths, vs. porosity plots. Figure 12 shows the elongation in the 2 in. gage length vs. porosity. The least squares best fit expression for this curve is:

$$\text{Per cent elongation} = \frac{1}{0.084 - 0.011\ (\%\ \text{loss in area})}$$

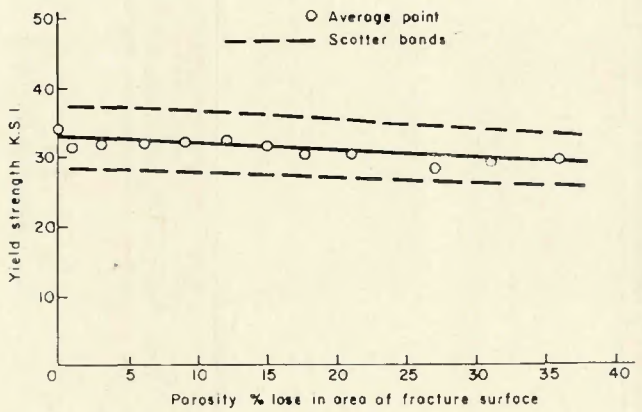

Fig. 11—Yield strength vs. porosity

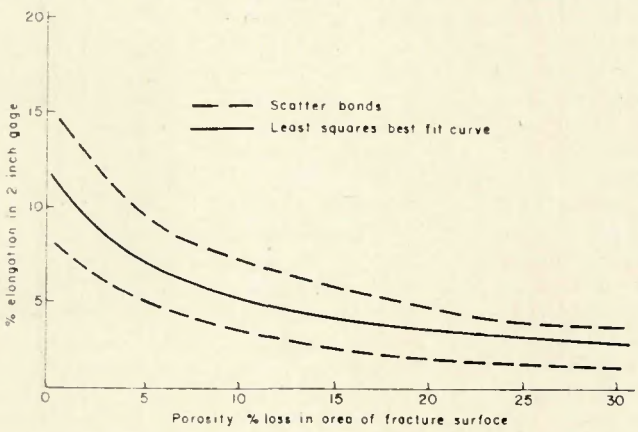

Fig. 12—Percent elongation in 2 in. gage vs. porosity

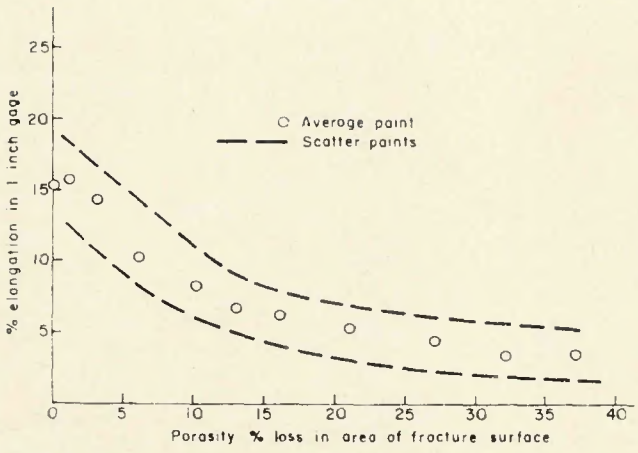

Fig. 13—Percent elongation in 1 in. gage vs. porosity

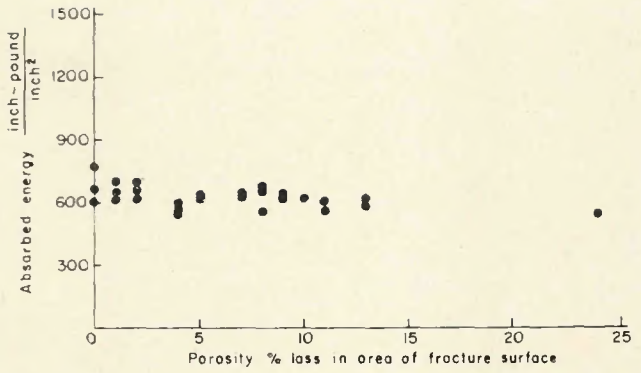

Fig. 14—Precracked Charpy test, energy absorbed vs. porosity

Scatter bands indicate the limits of variation for the data.

Figure 13 shows the percent elongation in the 1 in. gage length as a function of porosity. Scatter bands are plotted with average points.

The drop in both tensile strength and ductility with porosity is in agreement with Young and Dinsdales' findings that defects which seriously affect strength have a similar deleterious effect on ductility and that a consistent relationship exists between ultimate tensile strength and ductility for a given alloy.

From Fig. 10, the drop in tensile strength with porosity is proportional to the loss of sound weld metal in the plane of expected fracture. This is in agreement with recent results by Rudy and Rupert in which all pores were evaluated by a grid intercept method. In their study, analysis of porosity was also made by actual pore count of pores $\geq {}^{1}/_{64}$ in. diameter. Neglecting the fine pores, ${}^{1}/_{64}$ in. diameter, the tensile strength dropped off suddenly with small losses in area—10% porosity reducing strength over 30% for bead shaved, ${}^{1}/_{4}$ in. A. A. 2219-T87 transverse tensile specimen. Results of the grid intercept evaluation showed a much smaller in tensile strength for the bead on A.A. 2014-T6 transverse tensile specimens, A. A. 4043 filler metal—50% loss in area reducing strength approximately 30%.

Although the effects of porosity can be quantitatively stated from experimental results, the mechanism of failure is not precisely understood. Porosity is not significantly affecting the elastic properties of the material but is definitely affecting the plastic behavior of ductility of the material. Several viewpoints on ductile fracture can be cited to explain this phenomena.

Hayden et al.[17] comments that ductile fracture occurs after appreciable plastic deformation. They describe three distinct stages of ductile fracture in tension. These are:

1. The sample begins necking and cavities form in the necked region.
2. The cavities begin to coalesce into a crack in the center of the sample.
3. The crack proceeds outward toward the surface of the sample in a direction 45 deg to the tensile axis.

Hayden notes that cavities form usually at inclusions, and are elon-

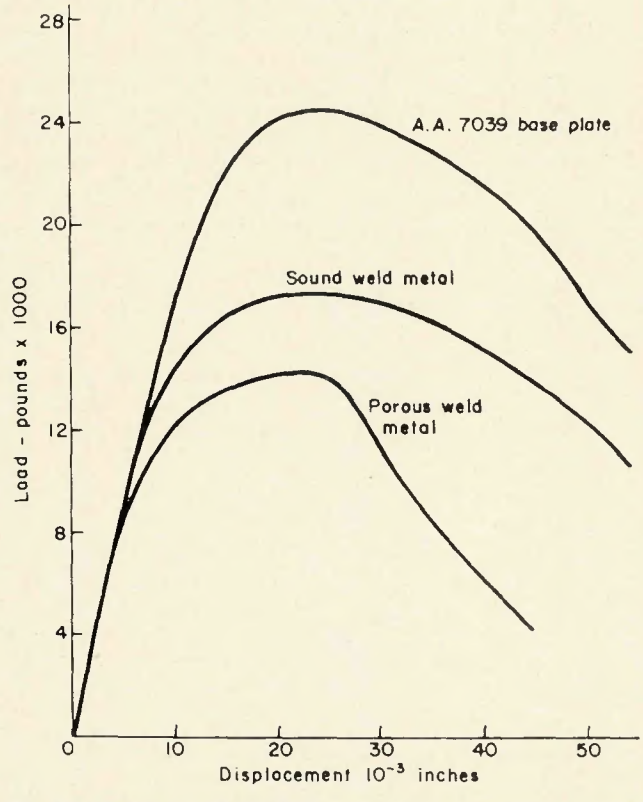

Fig. 15—Center notch fracture specimens, load-displacement curves

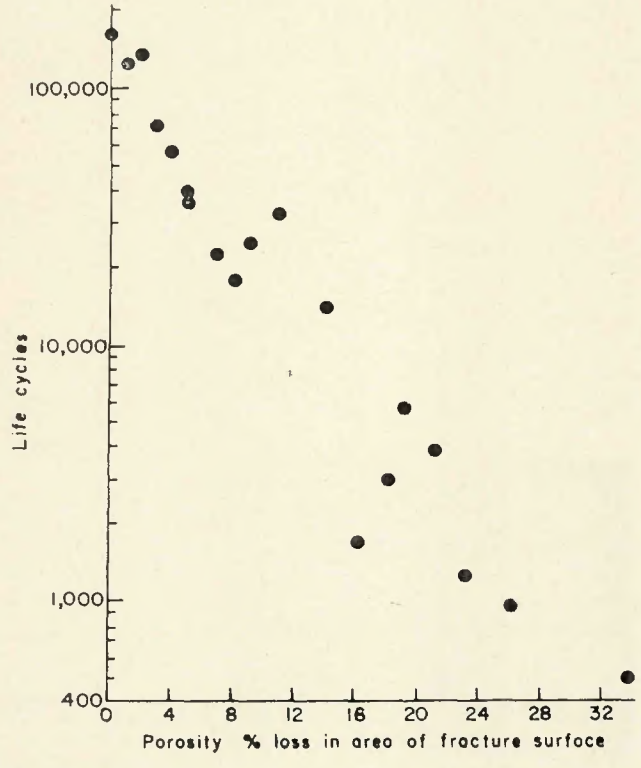

Fig. 16—Tension-tension fatigue, life cycles vs. porosity

gated in the direction of the maximum shear. Further, "the ductility of an alloy, as measured by the reduction of area at fracture, is greatly affected by the volume of voids or poorly bonded inclusions existent in the alloy." As an example, the ductility of copper, expressed as percentage reduction in cross-sectional area, is shown to drop from 80% to less than 10% with an increase in volume of voids from approximately zero to 8%. Hayden states that it is reasonable to expect similar behavior with other alloy systems.

Results of the elongation measurements seem consistent with Hayden's comments. Ductility is markedly reduced by small amounts of voids, and examination of pores in the plane of maximum shearing stress of fractured tensile specimens did indicate a slight elongation for those tensile specimens containing small amounts of porosity. No elongation was observed for highly porous weldments.

W. A. Backofen[18] states in his presentation on the "Metallurgical Aspects of Ductile Fracture" that cracks in plastic-working of materials result essentially from over extended flow. The cracks tend to occur along the rather well defined macroscopic boundaries between plastic and elastic fields. The boundary between these fields is abrupt and subject to very high shearing-strain rates. Backofen also notes that macroscopic discontinuities from fabrication by welding, forming, etc. are possible sources of strain concentration, setting up elastic-plastic boundaries and contributing to a shear failure. Crack nuclei may also be formed in the plastic zone adjacent to a pore by shearing a precipitate particle or the adjacent aluminum metal with high stresses induced by a dislocation pile-up. Hayden comments that such crack nuclei may produce sudden fracture at high stress and diminish the strain to fracture.

Whatever the exact mechanism for the reduced tensile strength and ductility, it is clear that fine pores, $\leq {}^{1}/_{64}$ in. in diameter, in the aluminum weld metal contribute to this property degradation and should be considered in any evaluation of porosity. More than 50% of the area loss in the porosity range 0 to 20% was from these fine pores.

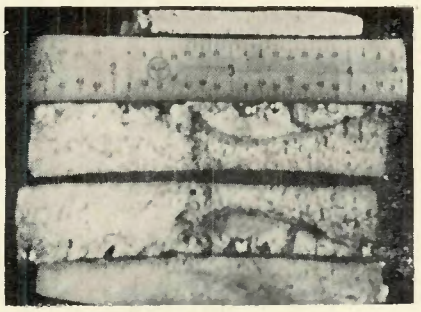

Fig. 17—Fatigue fracture surface

Toughness Tests

Results of precracked Charpy tests in Fig. 14 show that the weld metal's resistance to crack propagation under impact loading is not significantly affected by porosity. An embrittlement effect from hydrogen is not evident. Nearly all porosity on the fracture surfaces of the Charpy specimens were $\leq {}^{1}/_{64}$ in. in diameter.

The load-displacement curves for three center notched fracture specimens tested at WPAFB are shown in Fig. 15. These are for base metal (cracked with rolling direction), sound weld metal and porous weld metal. The weld metal samples were cracked in the center of the weld in the welding direction. Porosity loss in area for the porous sample was only 8% in the center of the weld but more than 25% near the edge of the weld. The tearing type failure for this sample moved from the center of the weld, after propagating approximately ${}^{1}/_{2}$ in., to this high porosity area.

Because of the vast amount of plastic flow and the absence of a popin, a valid plain strain value could not be obtained from the results. Relative toughnesses of the three test samples however, were computed using the K calibration by M. Isida for a finite-width center-cracked plate. As noted in ASTM STP 410 publication on *Plane Strain Fracture Toughness Testing*, this mathematical stress analysis was also performed by Forman and Kobayashi and by Alexander Mendelson. The results of all three analyses are in excellent agreement. Isida's K calibration, relating the crack tip stress intensity factor K to the applied load and specimen directions—including crack length, is shown below.

$$K = Y\frac{Pa^{1/2}}{BW}$$

where, K is the stress intensity factor in psi $(\text{in.})^{1/2}$; P is the load, for these calculations load was taken at 5% change in the reciprocal slope of the load-displacement recording; a is one-half the crack length, original crack length as measured from the fracture surfaces was used in these calculations; B is the original specimen thickness; W is the specimen width.

Y was obtained from the expression:

$$Y = 1.77\,[1 - 0.1(2a/W) + (2a/W)^2]$$

which is accurate within 1% over the range $2a/W$ between 0 and 0.6. The three values obtained with the above expression are for base metal:

$K_Q = 43{,}700$ psi $(\text{in.})^{1/2}$;
$K_Q = 24{,}400$ psi $(\text{in.})^{1/2}$;
$K_Q = 10{,}000$ psi $(\text{in.})^{1/2}$.

The K_Q values have significance only as relative toughness indications for the three samples considered. Significant embrittlement from porosity is not shown in Fig. 15. All three samples exhibited tearing type failures. Rapid crack propagation did not occur.

Fatigue

Results of the conventional (low speed) tension-tension fatigue tests are shown in Fig. 16. It is seen that small amounts of porosity significantly reduced the fatigue life of the weld metal. Individual pores and groups of pores serves as sites for crack initia-

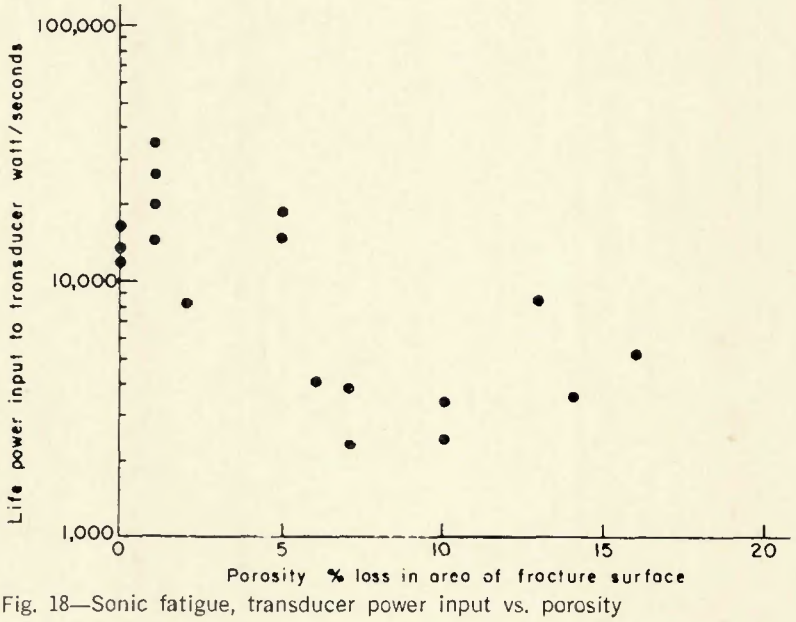

Fig. 18—Sonic fatigue, transducer power input vs. porosity

tion and growth as shown in Fig. 17.

The fatigue test was biased in that the stress for testing was based on the original cross-sectional area (assuming sound weld metal), not the actual load bearing cross-section—original areas minus the area lost to the porosity. In addition, the tensile strengths of the porous samples were lower than the tensile strengths of sound weld metal according to Fig. 10. Results of the fatigue test, however, are probably more realistic because of these two effects which occur naturally with porosity.

The fatigue life of the base metal is much greater than that of sound weld metal. A base metal sample under the same stress conditions, loaded transverse to the rolling direction, failed in the unpolished grip section after approximately 500,000 cycles.

The results of the sonic fatigue tests with specimens removed from the welded plates are plotted in Figs. 18 and 19. The power input to the transducer varied, 300 watts ± 100 watts, from test to test so both total power input in watt-seconds and the life cycles were plotted vs. porosity. In both cases, a drop in life with porosity is evident. This is in agreement with the results of the tension-tension fatigue tests.

There is considerable scatter in the data of Figs. 18 and 19. Variation in stress levels from test to test and fatigue initiating in the larger cross-sectional areas adjacent to the uniform reduced part of the sample are probable explanations for some of this variation. Although all fatigue tests were run at a constant input voltage to the transducer and at the apparent resonant frequency of the system, results of experiments showed that a slight change from this resonant frequency could significantly reduce the stress seen by the sample. Such a small change may have unknowingly reduced the stress levels for some of the tests. Failure out of the uniform reduced section of the sample occurred because the weld had not been centered properly in the sample.

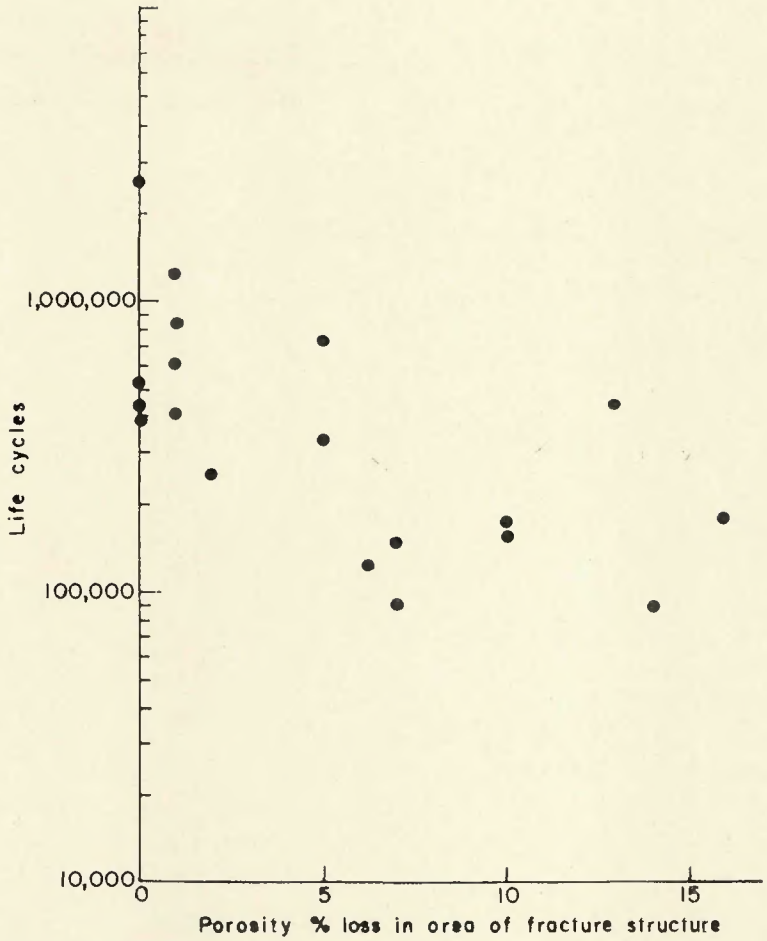

Fig. 19—Sonic fatigue, life cycles vs. porosity

The calibration curve for the stress at the center of the sample as a function of the applied voltage to the transducer at resonant frequency is shown in Fig. 20. These values were obtained using a single, foil strain gage and an oscilloscope. Static calibration was done on a tensile machine. Results of separate strain gage measurements on two samples were identical. Stresses at higher voltage were not obtained because the foil gages were damaged by the high strains. The stress wave pattern is shown in Fig. 21. Frequency of the stress wave was measured and found to be identical with that of the input voltage frequency to the transducer. No heating was observed in the test samples during testing. The transducer did not readily heat up either, since it

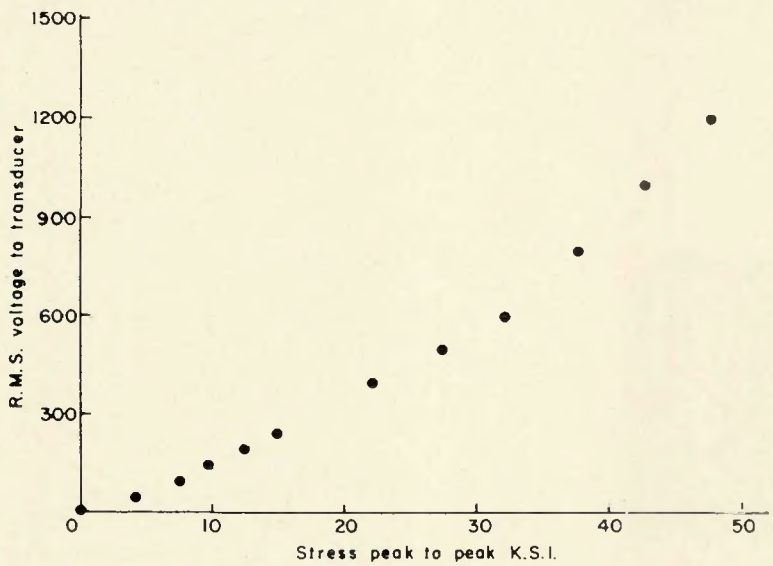

Fig. 20—Sonic fatigue calibration, voltage to transducer vs. stress

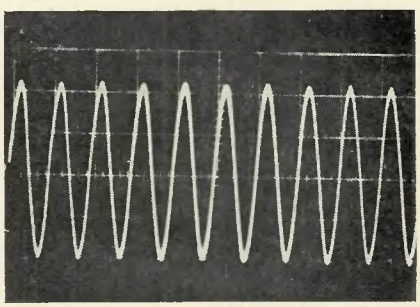
Fig. 21—Stress wave pattern in sonic fatigue sample

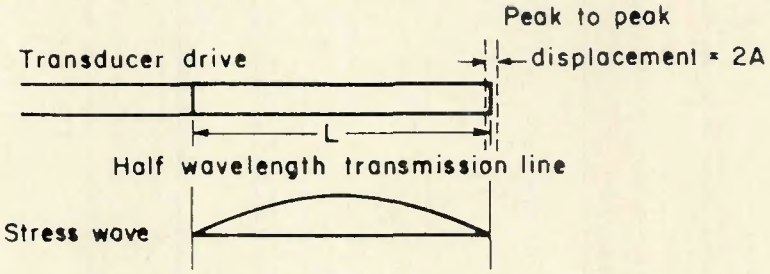

Fig. 22—Half wave length acoustic transmission line

was operating at only 600 v with power input of less than 10 percent of its rating.

The high stress levels, 50,000 psi peak to peak, in the center of the test sample can be explained, in part, by reviewing Dr. K. F. Graff's stress analysis for the maximum stress in a halfwave length acoustic transmission line being operated at resonant frequency with wavelength equal $2L$; refer to Fig. 22.

The relationships of parameters along the rod with time as a variable are, assuming elastic behavior:

1. Instantaneous displacement at any point along the rod:

$$u(x, t) = A\left(\cos\frac{\pi x}{L}\right)(\sin\omega t)$$

2. Instantaneous strain at any point along the rod:

$$\partial U/x = \Sigma = -A\frac{\pi}{L}\left(\sin\frac{\pi x}{L}\right)(\sin\omega t)$$

3. Instantaneous stress at any point along the rod:

$$\sigma = E\Sigma = -\frac{EA\pi}{L}\left(\sin\frac{\pi x}{L}\right)\sin\omega t$$

where E is Young's modulus and A is $^1/_2$ the peak to peak displacement of the free end of the transmission line. The maximum nodal stress is given by:

$$\text{Maximum nodal stress} = \frac{EA\pi}{L}$$

For aluminum, E is approximately 10,000 psi, with a tip displacement of 0.003 in. (L is approximately 10 in.) the maximum nodal stress would be on the order of 5000 psi or 10,000 psi peak to peak—one-fifth that observed in the sonic fatigue sample.

Tip displacement of 0.003 in. can be expected at the end of the P-11 transducer at high operating voltages (greater than approximately 2000 v). Therefore the stress calculation above is realistic for an aluminum rod of constant cross-section one-half wavelength long. As shown by the stress calculation and measurement, changing the aluminum sample from a uniform cross-section rod to the final sample shape of Fig. 3 resulted in a peak stress increase of over five times.

As a possible explanation of this increase in stress, consider the cross-sectional area of the sonic fatigue sample under static loading conditions, stress equals the load divided by cross-sectional area. Reducing the $^1/_2$ in. diameter sample to 0.280 in. at the center more than triples the static stress in this area. This area-loss concept could account for some of the observed stress increase. A second possible explanation is an increase in displacement. The tapered coupling nuts and tapered sections of the sample may amplify the displacement just as the "horn" of the transducer amplifies the piezoelectric ring movements.

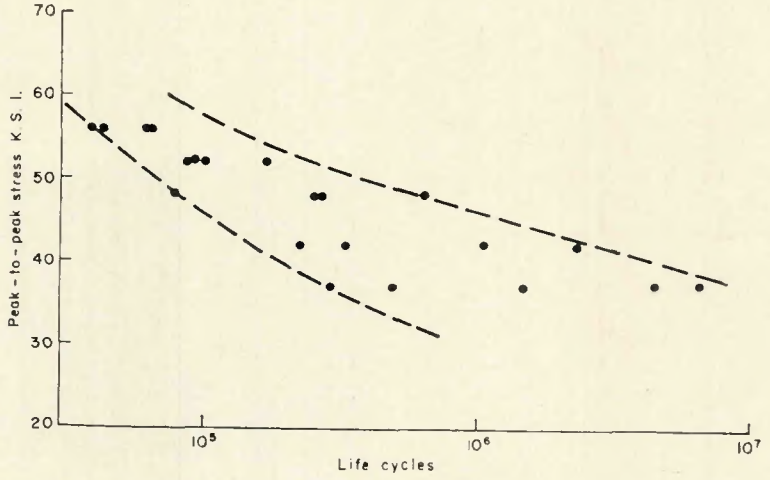

Fig. 23—Sonic fatigue S-N curve, 7039—T6151

As a further sonic fatigue test, test samples were removed from the $^1/_2$ in. thick A. A. 7039-T6151 base metal, rolling direction perpendicular to the longitudinal axis of the sample, and tested to determine the fatigue life at various stress levels (voltages). Sample size for these tests was the same as that shown in Fig. 3. By testing samples from the aluminum base metal, a more homogeneous material than the welded plate, test variables were reduced. Results of the tests are plotted in the S-N curve on Fig. 23. A sample was tested at 32,000 psi peak to peak stress for over 18 million cycles with no failure. This is consistent with plotted results. Results show less scatter for tests with the base material than for those with the welded plate.

Conclusions

The effects of the porosity in weld metal of A. A. 7039-T6151, $^1/_2$ in. plate, gas metal-arc welded in the flat position using A. A. 5039 filler metal, were determined experimentally. Porosity was obtained by moisture additions to helium shielding gas. All tests were conducted with weld bead removed by machining. The results indicate the following for porosity from 0 to approximately 40% as measured by the area loss in the fracture surface:

1. Porosity reduces the tranverse tensile strength of the weld metal an amount proportional to the area of sound metal lost in the fracture plane.
2. Yield strength of the weld metal is not significantly affected by porosity.
3. Ductility of the aluminum weld metal, as determined by percentage elongation measurements in tension tests, is sharply reduced by the presence of small amounts of porosity.
4. Fatigue life at high stress levels is markedly reduced by small amounts of porosity; these pores act as sites for crack initiation and growth.
5. Proportionately large amounts of fine porosity ($\leq {}^1/_{64}$ in. diameter) were encountered in the weld metal with the moisture addition contamination technique. This fine porosity affects the weld metal as noted in 1 through 4 and should be considered when evaluating porosity.
6. The results of the sonic fatigue test work suggests:
   (a) Fatigue testing at 10,000 c/s with the P-11 transducer offers many advantages over conventional type fatigue tests.
   (b) Further development work should be done in this area to refine the test apparatus and to correlate sonic fatigue results with conventional fatigue

data.

Acknowledgments

The authors wish to thank the staff of the Department of Welding Engineering at The Ohio State University of their help and advice. Thanks are also tendered to the Kaiser Aluminum and Chemical Corporation for the plate and wire used in this program as well as the technical advice of their personnel.

Also thanks are extended to the United States Air Force for their cooperation in permitting the use of fatigue and fracture toughness equipment of the Materials Laboratory at Wright Patterson Air Force Base as well as the support and technical advice of the laboratory personnel.

Bibliography

1. Saperstein, Z. P., Prescott, G. R., and Monroe, F. W., "Porosity in Aluminum Welds," WELDING JOURNAL, 44 (10), Research Suppl., 443-s to 453-s (1964).

2. Saperstein, Z. P., and Pollock, D. D., "Porosity Formation and Solidification Phenomena in Aluminum Welds," Paper presented at Aluminum Welding Symposium, NASA Marshall Space Flight Center, Huntsville, Alabama, July, 1964.

3. Brown, Hiram, "Aluminum Fabrication versus Environment Humidity," Paper for Presentation at NASA Seminar in Weld Porosity, Huntsville, Alabama.

4. Pfluger, A. R., and Lewis, R. E., editors, "Weld Imperfections," Proceedings of a Symposium at Lockheed Palo Alto Research Laboratory, September 19-21, 1966.

5. McCauley, R. B., "Standards for the Acceptance of Weld Defects," *Proceedings of the Fifth International Conference on Nondestructive Testing* (1967), p. 472-477.

6. Masubuchi, Koichi, "Integration of NASA-Sponsored Studies on Aluminum Welding," Redstone Scientific Information Center, September, 1967.

7. The Martin Marietta Company, results of NASA sponsored study NASA—11335, as noted from reference 9.

8. Rudy, J. F., Rupert, E. J., "Effects of Porosity on Mechanical Properties of Aluminum Welds," paper presented to American Welding Society, April, 1967.

9. Green, W. L., Hamad, M. F., and McCauley, R. B., "The Effects of Porosity on Mild Steel Welds," WELDING JOURNAL, 37 (5). Research Suppl., 206-s to 209-s (1958).

10. Bradley, J. W., "The Effects of Porosity on High-Strength Steel Welds." *Ibid.*, 43 (9), Research Suppl., 408-s to 414-s (1964).

11. Baysinger, F. R., "Observations on Porosity in Aluminum Weldments," Unpublished Paper, Kaiser Aluminum and Chemical Corporation, Spokane.

12. Dinsdale, W. O., and Young, J. G., "Significance of Defects in Aluminum Fusion Welds," Common Wealth Welding Conference Document M6, 1965.

13. Robinson, I. B., and Baysinger, F. R., "Welding Aluminum Alloy 7039," WELDING JOURNAL, 45 (10), Research Suppl., 433-s to 444-s (1966).

14. Mechanical Property Data 7039 Aluminum, issued by Air Force Materials Laboratory, Wright-Patterson Air Force Base, Ohio, prepared by Battelle Memorial Institute, Columbus, March, 1967.

15. Gibbs, F. E., "Development of Filler Metals for Welding Al-Zn-Mg Alloy 7039," WELDING JOURNAL, 45 (10), Research Suppl. 210-s to 226-s (1966).

16. Liptak, J. A., "Techniques for Welding 7039 Aluminum with Various Inert Gas Processes," *Ibid.*, 45 (12), Research Suppl., 561-s to 568-s (1966).

17. Moffatt, W. G., and Wulff, John, *The Structure and Properties of Materials*, Volume III—Mechanical Behavior, John Wiley & Sons, Inc., New York, 1965.